Ag@MoS2 core-shell heterostructure as SERS platform to reveal the hydrogen evolution active sites of single-layer MoS2

Chen, Junze; Liu, Guigao; Zhu, Yue-zhou; Su, Min; Yin, Pengfei; Wu, Xue-jun; Lu, Qipeng; Tan, Chaoliang; Zhao, Meiting; Liu, Zhengqing; Yang, Weimin; Li, Hai; Nam, Gwang-Hyeon; Zhang, Liping; Chen, Zhenhua; Huang, Xiao; Radjenovic, Petar M.; Huang, Wei; Tian, Zhong-qun; ...Zhang, Hua

2020

Chen, J., Liu, G., Zhu, Y.-z., Su, M., Yin, P., Wu, X.-j., ... Zhang, H. (2020). Ag@MoS2 core-shell heterostructure as SERS platform to reveal the hydrogen evolution active sites of single-layer MoS2. Journal of the American Chemical Society, 142(15), 7161–7167. doi:10.1021/jacs.0c01649

https://hdl.handle.net/10356/144116

https://doi.org/10.1021/jacs.0c01649

Ag@MoS_2 Core-Shell Heterostructure as SERS Platform to Reveal the Hydrogen Evolution Active Sites of Single-layer MoS_2

Junze Chen,[‡] Guigao Liu,[‡] Yuezhou Zhu,[‡] Min Su, Pengfei Yin, Xuejun Wu, Qipeng Lu, Chaoliang Tan, Meiting Zhao, Zhengqing Liu, Weimin Yang, Hai Li, Gwang-Hyeon Nam, Liping Zhang, Zhenhua Chen, Xiao Huang, Petar M. Radjenovic, Wei Huang, Zhongqun Tian, Jianfeng Li[*] and Hua Zhang[*]

ABSTRACT: Understanding the reaction mechanism for the catalytic process is essential to rational design and synthesis of the highly efficient catalyst. MoS_2 has been reported to be an efficient catalyst towards the electrochemical hydrogen evolution reaction (HER), but it still lacks direct experimental evidence to reveal the mechanism for MoS_2-catalyzed electrochemical HER process at atomic level. In this work, we develop a wet-chemical synthetic method to prepare the single-layer MoS_2-coated polyhedral Ag core-shell heterostructure (Ag@MoS_2) with tunable sizes as efficient catalysts for the electrochemical HER. The Ag@MoS_2 core-shell heterostructures are used as ideal platforms for the real-time surface-enhanced Raman spectroscopy (SERS) study owing to the strong electromagnetic field which is generated in the plasmonic Ag core. The *in situ* SERS results provide solid Raman spectroscopic evidence proving the S-H bonding formation on the MoS_2 surface during the HER process, suggesting that the S atom of MoS_2 is the catalytic active site for the electrochemical HER. It paves the way on the design and synthesis of heterostructures for exploring their catalytic mechanism at atomic level based on the *in situ* SERS measurement.

1. INTRODUCTION

Developing highly efficient catalysts for electrochemical hydrogen evolution reaction (HER) is critically important for clean and renewable energy application.[1,2] Recently, transition metal dichalcogenides (TMDs) have emerged as promising abundant and low-cost catalysts for HER.[3-5] As a landmark and classical example in TMDs, MoS_2 has received the most intensive attention due to its high chemical stability and excellent catalytic performance.[6-10] Understanding the HER mechanism of MoS_2 is very important to the rational design of MoS_2 and/or other Mo-S based molecule/cluster catalysts, as well as other TMD catalysts with superior HER performance. Although many efforts in both experiment and theory have been devoted to revealing the HER process on MoS_2,[11-17] the detailed mechanism as well as the identification of active sites are still not clear.

Capturing direct spectroscopic evidence of intermediates produced during catalytic processes is key to unravel the HER mechanism.[18,19] Surface-enhanced Raman spectroscopy (SERS) can provide surface-sensitive as well as chemical bond-specific signals at the atomic level, making it a powerful fingerprint spectroscopy which can *in situ* identify the active sites as well as the surface reaction intermediates during catalytic processes.[20-24] However, it still remains a challenge for *in situ* monitoring the HER process on MoS_2 since the lifetime of HER intermediates is short and the Raman signals on MoS_2 are undetectable due to its non/low-SERS active nature. Thus, the rational design and synthesis of core-shell heterostructure consisting of a SERS active core (such as Au, Ag and Cu) and an ultrathin MoS_2 shell is essential to extend the SERS study to MoS_2. Such core-shell structure might enable the direct Raman spectroscopic investigation on the HER process over MoS_2 due to the presence of SERS active core that generates a strong electromagnetic field to greatly enhance the signal of HER intermediates formed on the ultrathin MoS_2 shell. Unfortunately, the direct synthesis of such core-shell heterostructures with adjustable size and plasmonic property remains extremely challenging, especially for coating MoS_2 on the highly SERS-active Ag nanocrystals.

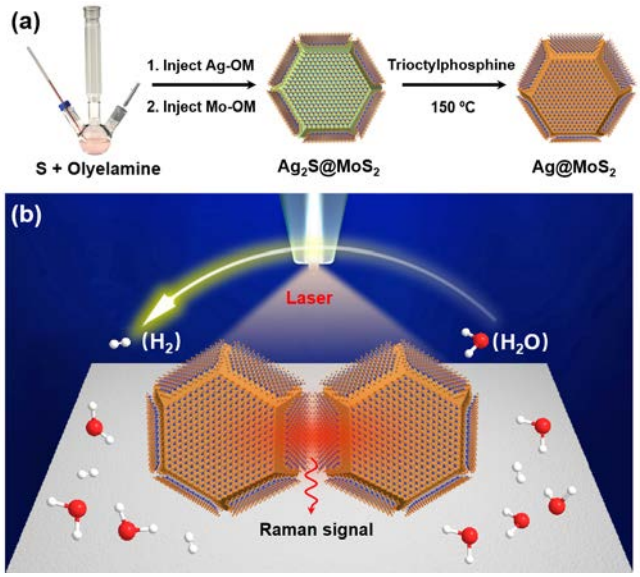

Figure 1. (a) Ag_2S@MoS_2 core-shell heterostructure was first synthesized by a one-pot method and then chemically transformed to Ag@MoS_2 by a heat treatment process in the presence of trioctylphosphine (TOP). Ag-OM and Mo-OM stand for the Ag-oleylamine and Mo-oleylamine stock solutions, respectively. (b) Scheme showing the EC-SERS study of the HER process on Ag@MoS_2. Once excited by a laser, the Ag@MoS_2 heterostructures can generate a strong electromagnetic field that can enhance Raman signals of reaction intermediates on MoS_2. The red ball represents the O atom. The white ball represents the H atom.

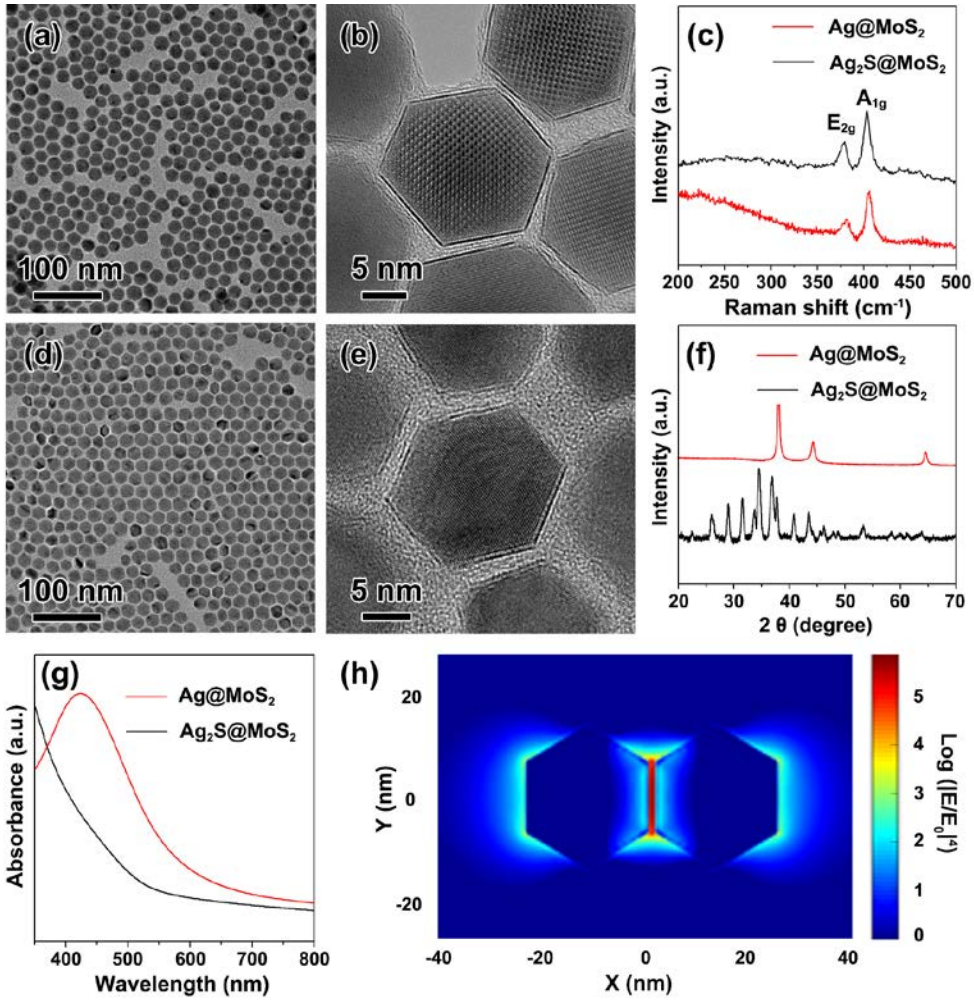

Figure 2. (a) The transmission electron microscopic (TEM) image, and (b) the high-resolution TEM (HRTEM) image of the synthesized $Ag_2S@MoS_2$ with size of 25.8±3.4 nm. (c) Raman Spectra of 25.8±3.4 nm $Ag_2S@MoS_2$ and 23.4±3.8 nm $Ag@MoS_2$. (d) The TEM, and (e) HRTEM images of the synthesized $Ag@MoS_2$ with size of 23.4±3.8 nm. (f) XRD patterns of 25.8±3.4 nm $Ag_2S@MoS_2$ and 23.4±3.8 nm $Ag@MoS_2$. (g) UV-vis absorption spectra of 25.8±3.4 nm $Ag_2S@MoS_2$ and 23.4±3.8 nm $Ag@MoS_2$ suspensions in toluene. (h) 3D-FDTD simulations of two 23.4 nm $Ag@MoS_2$ core-shell heterostructures on a SiO_2 substrate.

Herein, we develop a wet-chemical synthetic method for a controlled preparation of a series of $Ag@MoS_2$ core-shell heterostructures (Fig. 1a) via a wet-chemical method, which are then used as a new SERS platform to reveal the catalytic active site and study the mechanism of MoS_2 for HER (Fig. 1b). The obtained $Ag@MoS_2$ heterostructures show the size-dependent electrochemical activity towards the HER, which is superior to the pure MoS_2 nanosheets. Importantly, the strong electromagnetic field generated in the plasmonic Ag core enables the real-time visualization of intermediates on the MoS_2 surface during the electrochemical HER process in aqueous solution using *in situ* SERS technique (Fig. 1b). The Raman spectra clearly show the formation of S-H bonding during the HER process, directly evidencing that the S atom of MoS_2 is the catalytic active site towards the electrochemical HER.

2. RESULTS AND DISCUSSION

Synthesis and characterization of the as-synthesized $Ag@MoS_2$ core-shell heterostructures. Briefly, the $Ag@MoS_2$ core-shell heterostructures were obtained via a two-step wet-chemical synthetic method (see the Methods in the Supporting Information for experimental details). $Ag_2S@MoS_2$ core-shell heterostructures with different sizes are first synthesized by a one-pot method, which are then transferred to $Ag@MoS_2$ via a facile heat treatment process in the presence of trioctylphosphine (TOP, Fig. 1a). The low-resolution transmission electron microscopic (TEM) images (Fig. 2a and Fig. S1) show the synthesized $Ag_2S@MoS_2$ core-shell heterostructures with different sizes of 12.7±1.8, 20.2±2.9, 25.8±3.4 to 39.6±8.7 nm (Fig. S2). As shown in in Fig. 2b and Fig. S3, i.e. the high-resolution TEM (HRTEM) images, single-layer MoS_2 covered on the surface of Ag_2S is clearly observed, indicating the successful preparation of $Ag_2S@MoS_2$ core-shell heterostructures.

The crystal structures of the $Ag_2S@MoS_2$ with different sizes were investigated by the powder X-ray diffraction (XRD, shown in Fig. S4). All the peaks of $Ag_2S@MoS_2$ match well with those of monoclinic acanthite Ag_2S, indicating their pure Ag_2S phase. Furthermore, as shown in the Raman spectroscopy of $Ag_2S@MoS_2$ (Fig. 2c), two main Raman modes (A_{1g} and E_{2g}) can be clearly observed, indicating the formation of 2H-MoS_2, which was also confirmed by the X-ray photoelectron spectroscopy (XPS, shown in Fig. S5).

As reported previously, TOP can extract the sulfur from Ag_2S and reduce Ag^+ to the zero-valent Ag.[25-27] The $Ag_2S@MoS_2$ core-shell heterostructures with different sizes were successfully transformed to $Ag@MoS_2$ (Figs. 2d-e and Figs. S6-S7) by a facile heat treatment process in the presence of TOP (Fig. 1a). As shown in Fig. 2e and Fig. S7, the core-shell structure of $Ag_2S@MoS_2$ was

well-preserved in the obtained Ag@MoS_2, in which the single-layer MoS_2 was well maintained. After the transformation, the sizes of obtained Ag@MoS_2, i.e. 11.3±1.7, 18.1±2.6, 23.4±3.8 and 34.4±5.6 nm (Figs. 2d-e, Fig. S6-S8), slightly shrank, as compared to the corresponding original Ag_2S@MoS_2 (Figs. 2a-b, Figs. S1-S3). Moreover, the successful chemical transformation was also confirmed by XRD (Fig. 2f and Fig. S9), which indicates the formation of face-centered cubic (*fcc*) Ag in the obtained Ag@MoS_2. Furthermore, the 2H-MoS_2 still kept same, as proved by the Raman spectrum (Fig. 2c), and the UV-Vis spectrum of Ag@MoS_2 shows the localized surface plasmon resonance (LSPR) absorption of Ag at around 420 nm (Fig. 2g). All of the aforementioned results confirm the successful synthesis of Ag@MoS_2 core-shell heterostructures. The three-dimensional finite-difference time-domain (3D-FDTD) calculations (Fig. 2h, Fig. S10) suggest that the SERS enhancement factor of Ag@MoS_2 heterostructures increased with their size. Particularly, the Raman signal enhancement on the 'hot spot' between Ag@MoS_2 with the size of 34.4 nm was calculated to be increased by more than six orders of magnitude (Fig. S10d), suggesting that Ag@MoS_2 can serve as an ideal platform for detecting the reaction intermediates on the MoS_2-catalysed HER process using *in situ* electrochemical SERS (EC-SERS), as schematically shown in Fig. 1b.

Electrochemical activities of Ag@MoS_2 core-shell heterostructures. As known, the lifetime of reaction intermediates produced during HER is very short. In order to detect the intermediates by *in situ* EC-SERS, the Ag@MoS_2 should efficiently catalyze the HER to guarantee the sufficient formation of these intermediates. Therefore, prior to conducting *in situ* EC-SERS studies, the HER activity of Ag@MoS_2 with different sizes was first evaluated in 0.5 M H_2SO_4 electrolyte at room temperature (Fig. 3 and Figs. S11-S13). As comparison, the commercial Pt/C (20 wt%), and the synthesized MoS_2 nanosheets and Ag nanocrystals (Fig. S14, please see Supporting Information for details) were also tested

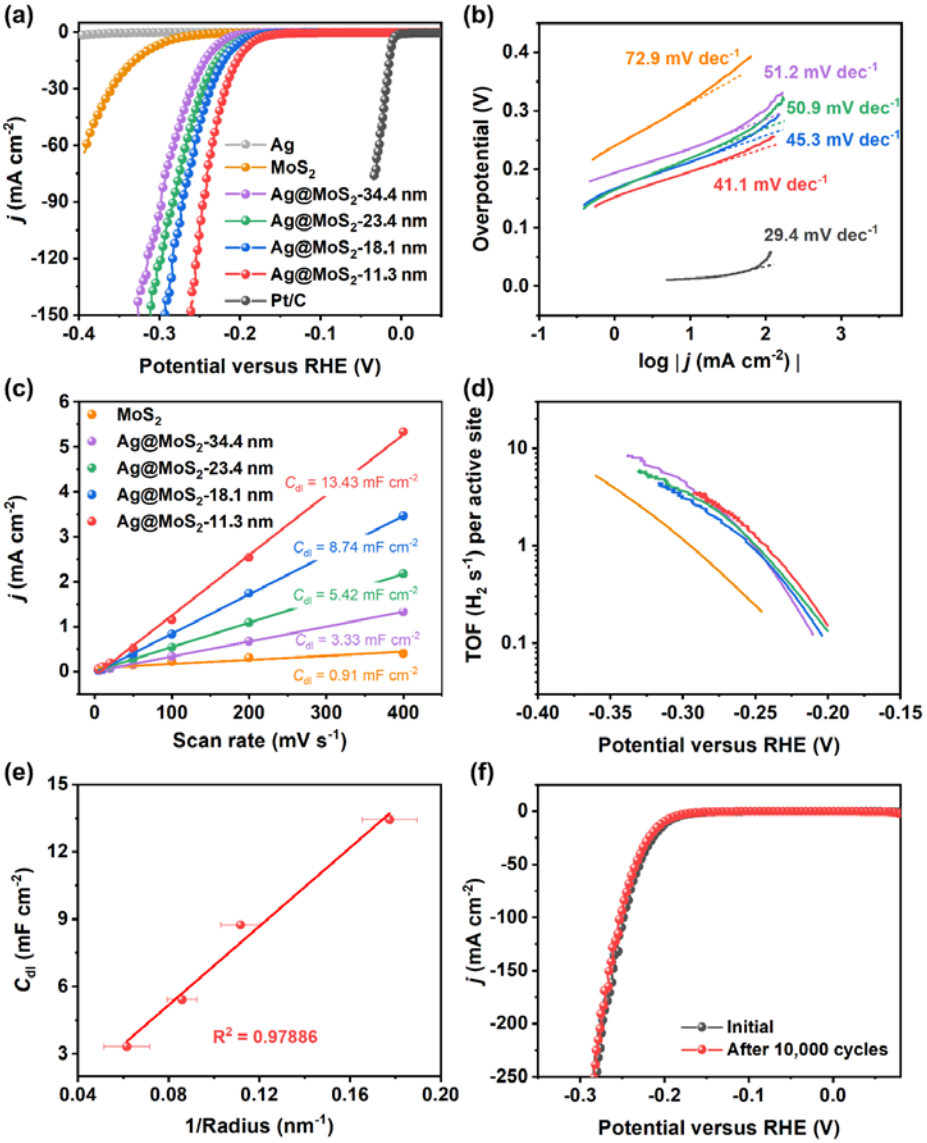

Figure 3. (a) LSV curves for HER measured on the commercial Pt/C, Ag nanocrystals, MoS_2 nanosheets, and Ag@MoS_2 with different sizes. (b) The Tafel plots derived from the LSV curves in (a). (c) The plot of capacitive current density versus scan rate. The electrochemical double-layer capacitances (C_{dl}), measured on MoS_2 nanosheets and Ag@MoS_2 with different sizes, correspond to the slopes of the linear fits to their data. (d) TOF values of MoS_2 nanosheets and Ag@MoS_2 with different sizes, calculated by using 0.06 mF cm^{-2} as the specific capacitance for the flat MoS_2 electrode. (e) The plot C_{dl} of Ag@MoS_2 heterostructures versus 1/radius. (f) Durability test on Ag@MoS_2 with size of 11.3±1.7 nm. The polarization curves were recorded at sweeping rate of 5 mV s^{-1} before and after 10,000 potential cycles.

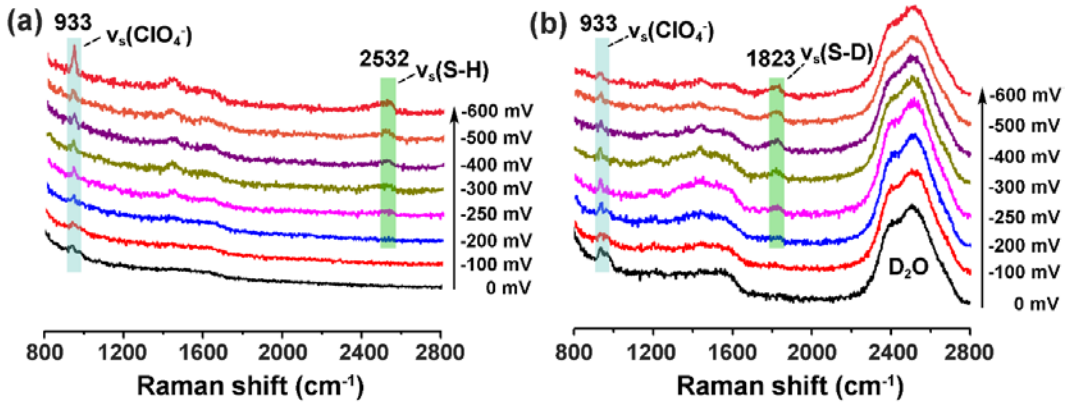

Figure 4. (a) EC-SERS spectra of HER on Ag@MoS_2 with size of 23.4±3.8 nm in 0.1 M $HClO_4$ electrolyte. (b) EC-SERS spectra of HER on Ag@MoS_2 with size of 23.4±3.8 nm in a 0.1 M $DClO_4$ electrolyte. The arrows show the potential scanning direction. All potentials were calibrated to the reversible hydrogen electrode (RHE).

under same experimental conditions. As shown in the *i*R-corrected linear sweep voltammograms (LSV) in Fig. 3a, all Ag@MoS_2 heterostructures exhibit much higher catalytic activity towards HER compared to MoS_2 nanosheets, and Ag nanocrystals show no measurable HER activity within the investigated potential window. It clearly indicates that the superior activity of Ag@MoS_2 arises from the MoS_2 shell rather than the Ag core, making it an ideal platform to investigate HER process on MoS_2 by *in situ* EC-SERS without any contribution from Ag. Importantly, the HER activity of Ag@MoS_2 is size-dependent. The LSV curves of Ag@MoS_2 shifted gradually to more negative potentials with the size increasing (Fig. 3a). To achieve the current density of 10 mA cm^{-2}, the overpotentials required for Ag@MoS_2 with sizes of 11.3±1.7, 18.1±2.6, 23.4±3.8 and 34.4±5.6 nm are 195.7, 212.6, 218.8 and 235.3 mV, respectively (Fig. S15).

Furthermore, the kinetic behavior of Ag@MoS_2 for HER was analyzed by the Tafel slope. Compared to the MoS_2 nanosheets (72.9 mV dec^{-1}), all Ag@MoS_2 heterostructures show much lower Tafel slopes with values ranging from 41.1 to 51.2 mV dec^{-1} (Fig. 3b), reflecting their superior HER kinetics. Furthermore, the observed Tafel slopes for Ag@MoS_2 heterostructures suggest that their HER proceeds via the Volmer-Heyrovsky mechanism that involves electrochemical desorption as the rate-determining step.[28,29]

The electrochemically active surface area (ECSA) of Ag@MoS_2 was estimated by calculating the electrochemical double-layer capacitance (C_{dl}), which is linearly proportional to the effective active surface area (Supporting Note 1).[30] As shown in Fig. 3c and Figs. S16-S20, the C_{dl} values of Ag@MoS_2 heterostructures with sizes of 11.3±1.7, 18.1±2.6, 23.4±3.8 and 34.4±5.6 nm were calculated to be 13.43, 8.74, 5.42 and 3.33 mF cm^{-2}, respectively, which are much greater compared to MoS_2 nanosheets (0.91 mF cm^{-2}). Based on a specific capacitance (C_s) of 0.06 mF cm^{-2} for the flat MoS_2 surface,[31] the roughness factors of Ag@MoS_2 heterostructures with sizes of 11.3±1.7, 18.1±2.6, 23.4±3.8 and 34.4±5.6 nm, as well as MoS_2 nanosheets were estimated to be 223.8, 145.7, 90.3, 55.5, and 15.2, respectively (Supporting Note 1 and Fig. S21). These results suggest that the unique core-shell heterostructure of Ag@MoS_2 results in a remarkable increase in active sites of MoS_2, leading to the enhanced HER performance. Moreover, the turnover frequency (TOF) and the specific activities for Ag@MoS_2 and MoS_2 were also estimated (Supporting Note 2). As shown in Fig. 3d and Fig. S22, at all potentials, the Ag@MoS_2 heterostructures exhibit much larger TOF values and specific activities than does the MoS_2 nanosheet, suggesting that the intrinsic catalytic activity of MoS_2 for HER could be dramatically promoted in Ag@MoS_2. Such high intrinsic activity of Ag@MoS_2 might be attributed to the single-layer nature of the MoS_2 shell (Fig. 2e) and the low charge transfer resistance (*R*ct) due to the high conductivity of Ag core (Fig. S13b). Here, it is worth mentioning that Ag@MoS_2 heterostructures with different sizes possess similar TOF values at the same potential (Fig. 3d), suggesting that the intrinsic catalytic activity of the single-layer MoS_2 shell was well maintained, which is independent of the size of Ag@MoS_2. The nearly linear relationship between the *C*dl and 1/radius of Ag@MoS_2 (Fig. 3e) reflects that this unique heterostructure enables the easy tuning of the ECSA and thus the HER activity of MoS_2 by the size of Ag@MoS_2. Furthermore, the HER durability of Ag@MoS_2 was also evaluated. As shown in Fig. 3f and Fig. S23, all Ag@MoS_2 heterostructures with different sizes exhibit superb stability with negligible shifts in their polarization curves after 10,000 potential cycles.

EC-SERS measurements of Ag@MoS_2 core-shell heterostructures. The *in situ* EC-SERS was used to monitor the HER process in 0.1 M $HClO_4$ electrolyte. Fig. 4 and Figs. S24-S29 show the EC-SERS spectra of HER on various Ag@MoS_2 heterostructures with different sizes, Ag nanocrystals, MoS_2 nanosheets, and the mixture of Ag nanocrystals and MoS_2 nanosheets, recorded in the potential range from 0 to -600 mV. Despite the highest activity towards HER (Fig. 3a), Ag@MoS_2 with size of 11.3±1.7 nm shows almost no Raman signal during the HER process (Fig. S24). This could be attributed to the low SERS enhancement factor as shown by the 3D-FDTD simulations in Fig. S10a. Surprisingly, the SERS signal during HER recorded on Ag@MoS_2 with size of 34.4±5.6 nm is also weak (Fig. S26), although it exhibits the highest SERS enhancement ability (Fig. S10d). This may be due to its relatively low activity towards HER (Fig. 3a), leading to the inefficient production of intermediates. The strongest Raman signal during HER was obtained on the Ag@MoS_2 with size of 23.4±3.8 nm as a result of the combination of the SERS enhancement ability (Fig. S10c) and the HER activity (Fig. 3a). As shown in Fig. 4a, during the potential going down from 0 to -200 mV, except the peak at 933 cm^{-1} belonging to $\nu_s(ClO^{4-})$[32], no other Raman signals ranging from 800 to 2800 cm^{-1} was observed. When the potential reaches -250 mV, an obvious Raman peak located at ca. 2532 cm^{-1} appears and its intensity increases as the potential further decreases to -600 mV. In contrast, such Raman peak was not detected on the Ag nanocrystals with similar size of 20.3±3.6 (Fig. S14b and Fig. S27), MoS_2 nanosheets (Fig. S14a and Fig. S28), and the mixture of Ag nanocrystals and MoS_2 nanosheets (Fig. S29). The band detected at 2532 cm^{-1} is ascribed to the stretching vibration of S-H bonds, ν(S-H) (ref.[33]), indicating that the H atom is directly bonded to the S

atom of MoS_2 during the HER. The assignment of the peak at 2532 cm^{-1} to ν(S-H) can be further confirmed by the deuterium isotopic substitution experiment. As shown in Fig. 4b, the peak around 2532 cm^{-1} observed in the 0.1 M $HClO_4$ electrolyte shifts to a lower wavenumber of around 1823 cm^{-1} in the 0.1 M $DClO_4$ electrolyte. The result of frequency decrease is in good agreement with an isotopic shift factor of 1.39, as calculated by the harmonic oscillator model. Furthermore, the EC-SERS measurement on Ag@MoS_2 with size of 23.4±3.8 nm was also performed in the 0.5 M H_2SO_4 electrolyte. As illustrated in Fig. S30, the Raman peak of ν(S-H) at 2532 cm^{-1} was also detected during the HER, well consistent with the aforementioned result obtained in the 0.1 M $HClO_4$ electrolyte (Fig. 4a). Importantly, it is worth mentioning that the vibrational signals, ν(Mo-H), between 1714 and 1942 cm^{-1} (refs.[34,35]) have not been observed in the EC-SERS measurements (Fig. 4a, Figs. S24-S30). Based on detailed fingerprint information mentioned above, it is concluded that the S atom of MoS_2 is the catalytic active site for the HER. Albeit different from our crystalline MoS_2 nanosheets, the S atoms in amorphous MoS_X (ref.[36]) were also confirmed to be the active sites for HER.

3. CONCLUSION

In summary, in order to study the HER mechanism on MoS_2, we have successfully synthesized a series of Ag@MoS_2 core-shell heterostructures with different sizes. These heterostructures showed size-dependent HER performances and SERS enhancement abilities. The EC-SERS was used to investigate the HER process on the single-layer MoS_2 surface of Ag@MoS_2. Direct spectral evidence of the formation of S-H bonding suggests that the S atoms of MoS_2 are the HER catalytic active sites. Our work not only provides a strategy for preparation of TMD-based core-shell heterostructures, but also lays the foundation for future studies of the HER mechanism on MoS_2 by *in situ* SERS, which could pave the way to the rational design and synthesis of the highly efficient catalysts for water splitting. Our strategy may also be applicable to *in situ* probe other catalytic processes (such as organic conversion, CO_2 reduction, nitrogen reduction, etc.) over different transition metal dichalcogenide catalysts.

ASSOCIATED CONTENT

Supporting Information

The Supporting Information is available free of charge on the ACS Publications website.

Experimental details and characterization data, including Figures S1-S30.

AUTHOR INFORMATION

Corresponding Author

Hua Zhang - *Department of Chemistry, City University of Hong Kong, Hong Kong, China. Hong Kong Branch of National Precious Metals Material Engineering Research Center (NPMM), City University of Hong Kong, Hong Kong, China.*

Email: hua.zhang@cityu.edu.hk

Jianfeng Li - *State Key Laboratory of Physical Chemistry of Solid Surfaces, iChEM, Department of Physics, College of Chemistry and Chemical Engineering, and College of Energy, Xiamen University, Xiamen, China.*

Email: Li@xmu.edu.cn

Author Contributions

Junze Chen - *Center for Programmable Materials, School of Materials Science and Engineering, Nanyang Technological University, 50 Nanyang Avenue, Singapore 639798, Singapore.*

Guigao Liu - *Center for Programmable Materials, School of Materials Science and Engineering, Nanyang Technological University, 50 Nanyang Avenue, Singapore 639798, Singapore.*

Yuezhou Zhu - *State Key Laboratory of Physical Chemistry of Solid Surfaces, iChEM, Department of Physics, College of Chemistry and Chemical Engineering, and College of Energy, Xiamen University, Xiamen, China.*

Min Su - *State Key Laboratory of Physical Chemistry of Solid Surfaces, iChEM, Department of Physics, College of Chemistry and Chemical Engineering, and College of Energy, Xiamen University, Xiamen, China.*

Pengfei Yin - *Department of Chemistry, City University of Hong Kong, Hong Kong, China. Center for Programmable Materials, School of Materials Science and Engineering, Nanyang Technological University, 50 Nanyang Avenue, Singapore 639798, Singapore.*

Xuejun Wu - *State Key Laboratory of Coordination Chemistry, School of Chemistry and Chemical Engineering, Nanjing University, Nanjing 210023, China.*

Qipeng Lu - *Center for Programmable Materials, School of Materials Science and Engineering, Nanyang Technological University, 50 Nanyang Avenue, Singapore 639798, Singapore.*

Chaoliang Tan - *Center for Programmable Materials, School of Materials Science and Engineering, Nanyang Technological University, 50 Nanyang Avenue, Singapore 639798, Singapore.*

Meiting Zhao - *Center for Programmable Materials, School of Materials Science and Engineering, Nanyang Technological University, 50 Nanyang Avenue, Singapore 639798, Singapore.*

Zhengqing Liu - *Center for Programmable Materials, School of Materials Science and Engineering, Nanyang Technological University, 50 Nanyang Avenue, Singapore 639798, Singapore.*

Weimin Yang - *State Key Laboratory of Physical Chemistry of Solid Surfaces, iChEM, Department of Physics, College of Chemistry and Chemical Engineering, and College of Energy, Xiamen University, Xiamen, China.*

Hai Li - *Institute of Advanced Materials (IAM), Nanjing Tech University (NanjingTech), 30 South Puzhu Road, Nanjing 211816, China.*

Gwang-Hyeon Nam - *Center for Programmable Materials, School of Materials Science and Engineering, Nanyang Technological University, 50 Nanyang Avenue, Singapore 639798, Singapore.*

Liping Zhang - *Center for Programmable Materials, School of Materials Science and Engineering, Nanyang Technological University, 50 Nanyang Avenue, Singapore 639798, Singapore.*

Zhenhua Chen - *Jinzhou Medical University, Songpo Road, Jinzhou 121001, China.*

Xiao Huang - *Institute of Advanced Materials (IAM), Nanjing Tech University (NanjingTech), 30 South Puzhu Road, Nanjing 211816, China.*

Petar M. Radjenovic - *State Key Laboratory of Physical Chemistry of Solid Surfaces, iChEM, Department of Physics, College of Chemistry and Chemical Engineering, and College of Energy, Xiamen University, Xiamen, China.*

Wei Huang - *Institute of Advanced Materials (IAM), Nanjing Tech University (NanjingTech), 30 South Puzhu Road, Nanjing 211816, China. The Key Laboratory for Organic Electronics and Information Displays, Institute of Advanced Materials, Nanjing University of Posts and Telecommunications, Nanjing, China. Shaanxi Institute of Flexible Electronics, Northwestern Polytechnical University, Xi'an, China.*

Zhongqun Tian - *State Key Laboratory of Physical Chemistry of Solid Surfaces, iChEM, Department of Physics, College of Chemistry and Chemical Engineering, and College of Energy, Xiamen University, Xiamen, China.*

Author Contributions

‡ J.C., G.L. and Y.Z. contributed equally.

Notes

The authors declare no competing financial interest.

ACKNOWLEDGMENT

This research was financially supported by MOE under AcRF Tier 1 (Project No. 2017-T1-002-119) and AcRF Tier 2 (Project No. MOE2017-T2-1-162; MOE2016-T2-2-103) in Singapore, NTU's Start-Up Grant (Project No. M4081296.070.500000), and NSFC (21775127 and 21522508). H.Z. acknowledges the financial support from ITC via the Hong Kong Branch of National Precious Metals Material Engineering Research Center (NPMM), and the grants (Project No. 9380100, 9610478 and 1886921) in the City University of Hong Kong.

REFERENCES

(1) Roger, I.; Shipman, M.; Symes, M. Earth-abundant catalysts for electrochemical and photoelectrochemical water splitting. *Nat. Rev. Chem.* **2017**, *1*, 0003.

(2) Subbaraman, R.; Tripkovic, D.; Strmcnik, D.; Chang, K.-C.; Uchimura, M.; Paulikas, A. P.; Stamenkovic, V.; Markovic, N. M. Enhancing hydrogen evolution activity in water splitting by tailoring Li^+ -$Ni(OH)_2$-Pt interfaces. *Science* **2011**, *334*, 1256-1260.

(3) Chhowalla, M.; Shin, H. S.; Eda, G.; Li, L.-J.; Loh, K. P.; Zhang, H. The chemistry of ultra-thin transition metal dichalcogenide nanosheets. *Nat. Chem.* **2013**, *5*, 263-275.

(4) Tan, C.; Cao, X.; Wu, X.-J.; He, Q.; Yang, J.; Zhang, X.; Chen, J.; Zhao, W.; Han, S.; Nam, G.-H. Sindoro, M.; Zhang, H. Recent advances in ultrathin two-dimensional nanomaterials. *Chem. Rev.* **2017**, *117*, 6225-6331.

(5) Xu, M.; Liang, T.; Shi, M.; Chen, H. Graphene-like two-dimensional materials. *Chem. Rev.* **2013**, *113*, 3766-3798.

(6) Voiry, D.; Salehi, M.; Silva, R.; Fujita, T.; Chen, M.; Asefa, T.; Shenoy, V. B.; Eda, G.; Chhowalla, M. Conducting MoS_2 nanosheets as catalysts for hydrogen evolution reaction. *Nano Lett.* **2013**, *13*, 6222-6227.

(7) Li, Y.; Wang, H.; Xie, L.; Liang, Y.; Hong, G.; Dai, H. MoS_2 nanoparticles grown on graphene: an advanced catalyst for the hydrogen evolution reaction. *J. Am. Chem. Soc.* **2011**, *133*, 7296-7299.

(8) Kibsgaard, J.; Chen, Z.; Reinecke, B. N.; Jaramillo, T. F. Engineering the surface structure of MoS_2 to preferentially expose active edge sites for electrocatalysis. *Nat. Mater.* **2012**, *11*, 963-969.

(9) Yu, Y.; Nam, G.-H.; He, Q.; Wu, X.-J.; Zhang, K.; Yang, Z.; Chen, J.; Ma, Q.; Zhao, M.; Liu, Z.; Gu, L.; Du, Y.; Huang, W.; Zhang, H. High phase-purity 1T′-MoS_2-and 1T′-$MoSe_2$-layered crystals. *Nat. Chem.* **2018**, *10*, 638-643.

(10) Tsai, C.; Li, H.; Park, S.; Park, J.; Han, H. S.; Nørskov, J. K.; Zheng, X.; Abild-Pedersen, F. Electrochemical generation of sulfur vacancies in the basal plane of MoS_2 for hydrogen evolution. *Nat. Commun.* **2017**, *8*, 15113.

(11) Jaramillo, T. F.; Jørgensen, K. P.; Bonde, J.; Nielsen, J. H.; Horch, S.; Chorkendorff, I. Identification of active edge sites for electrochemical H_2 evolution from MoS_2 nanocatalysts. *Science* **2007**, *317*, 100-102.

(12) Voiry, D.; Fullon, R.; Yang, J.; e Silva, C. d. C. C.; Kappera, R.; Bozkurt, I.; Kaplan, D.; Lagos, M. J.; Batson, P. E.; Gupta, G.; Mohite, A. D.; Dong, L.; Er, D.; Shenoy, V. B.; Asefa, T.; Chhowalla, M. The role of electronic coupling between substrate and 2D MoS_2 nanosheets in electrocatalytic production of hydrogen. *Nat. Mater.* **2016**, *15*, 1003-1009.

(13) Hinnemann, B.; Moses, P. G.; Bonde, J.; Jørgensen, K. P.; Nielsen, J. H.; Horch, S.; Chorkendorff, I.; Nørskov, J. K. Biomimetic hydrogen evolution: MoS_2 nanoparticles as catalyst for hydrogen evolution. *J. Am. Chem. Soc.* **2005**, *127*, 5308-5309.

(14) Zhang, J.; Wu, J.; Guo, H.; Chen, W.; Yuan, J.; Martinez, U.; Gupta, G.; Mohite, A.; Ajayan, P. M.; Lou, J. Unveiling active sites for the hydrogen evolution reaction on monolayer MoS_2. *Adv. Mater.* **2017**, *29*, 1701955.

(15) Huang, Y.; Nielsen, R. J.; Goddard III, W. A.; Soriaga, M. P. The reaction mechanism with free energy barriers for electrochemical dihydrogen evolution on MoS_2. *J. Am. Chem. Soc.* **2015**, *137*, 6692-6698.

(16) Huang, Y.; Nielsen, R. J.; Goddard III, W. A. Reaction mechanism for the hydrogen evolution reaction on the basal plane sulfur vacancy site of MoS_2 using grand canonical potential kinetics. *J. Am. Chem. Soc.* **2018**, *140*, 16773-16782.

(17) Tang, Q.; Jiang, D.-E. Mechanism of hydrogen evolution reaction on 1T-MoS_2 from first principles. *ACS Catal.* **2016**, *6*, 4953-4961.

(18) Huang, Y.; Kooyman, P.; Koper, M. Intermediate stages of electrochemical oxidation of single-crystalline platinum revealed by *in situ* Raman spectroscopy. *Nat. Commun.* **2016**, *7*, 12440.

(19) Dong, J.-C.; Zhang, X.-G.; Briega-Martos, V.; Jin, X.; Yang, J.; Chen, S.; Yang, Z.-L.; Wu, D.-Y.; Feliu, J. M.; Williams, C. T.; Tian, Z.-Q.; Li, J.-F. *In situ* Raman spectroscopic evidence for oxygen reduction reaction intermediates at platinum single-crystal surfaces. *Nat. Energy* **2019**, *4*, 60-67.

(20) Li, J.-F.; Zhang, Y.-J.; Ding, S.-Y.; Panneerselvam, R.; Tian, Z.-Q. Core-shell nanoparticle-enhanced Raman spectroscopy. *Chem. Rev.* **2017**, *117*, 5002-5069.

(21) Li, C.-Y.; Dong, J.-C.; Jin, X.; Chen, S.; Panneerselvam, R.; Rudnev, A. V.; Yang, Z.-L.; Li, J.-F.; Wandlowski, T.; Tian, Z.-Q. *In Situ* monitoring of electrooxidation processes at gold single crystal surfaces using shell-isolated nanoparticle-enhanced Raman spectroscopy. *J. Am. Chem. Soc.* **2015**, *137*, 7648-7651.

(22) Moskovits, M. Surface-enhanced spectroscopy. *Rev. Mod. Phys.* **1985**, *57*, 783-826.

(23) Wang, Y. H.; Le, J. B.; Li, W. Q.; Wei, J.; Radjenovic, P. M.; Zhang, H.; Zhou, X. S.; Cheng, J.; Tian, Z. Q.; Li, J. F. *In situ* spectroscopic insight into the origin of the enhanced performance of bimetallic nanocatalysts towards ORR. *Angew. Chem. Int. Ed.* **2019**, *58*, 16062-16066.

(24) Li, C.-Y.; Le, J.-B.; Wang, Y.-H.; Chen, S.; Yang, Z.-L.; Li, J.-F.; Cheng, J.; Tian, Z.-Q. *In situ* probing electrified interfacial water structures at atomically flat surfaces. *Nat. Mater.* **2019**, *18*, 697-701.

(25) Sines, I. T.; Schaak, R. E. Phase-selective chemical extraction of selenium and sulfur from nanoscale metal chalcogenides: a general strategy for synthesis, purification, and phase targeting. *J. Am. Chem. Soc.* **2011**, *133*, 1294-1297.

(26) Zhou, J.; Huang, F.; Xu, J.; Wang, Y. Converting Ag_2S-CdS and Ag_2S-ZnS into Ag-CdS and Ag-ZnS nanoheterostructures by selective extraction of sulfur. *Chem. Asian J.* **2014**, *9*, 3287-3290.

(27) Han, S.-K.; Gu, C.; Gong, M.; Yu, S.-H. A trialkylphosphine-driven chemical transformation route to Ag-and Bi-based chalcogenides. *J. Am. Chem. Soc.* **2015**, *137*, 5390-5396.

(28) Shinagawa, T.; Garcia-Esparza, A. T.; Takanabe, K. Insight on Tafel slopes from a microkinetic analysis of aqueous electrocatalysis for energy conversion. *Sci. Rep.* **2015**, *5*, 13801.

(29) Ledezma-Yanez, I.; Wallace, W. D. Z.; Sebastián-Pascual, P.; Climent, V.; Feliu, J. M.; Koper, M. T. Interfacial water reorganization as a pH-dependent descriptor of the hydrogen evolution rate on platinum electrodes. *Nat. Energy* **2017**, *2*, 17031.

(30) Gao, M.-R.; Chan, M. K.; Sun, Y. Edge-terminated molybdenum disulfide with a 9.4-Å interlayer spacing for electrochemical hydrogen production. *Nat. Commun.* **2015**, *6*, 7493.

(31) Benck, J. D.; Chen, Z.; Kuritzky, L. Y.; Forman, A. J.; Jaramillo, T. F. Amorphous molybdenum sulfide catalysts for electrochemical hydrogen production: insights into the origin of their catalytic activity. *ACS Catal.* **2012**, *2*, 1916-1923.

(32) Ratcliffe, C. I.; Irish, D. E. Vibrational spectral studies of solutions at elevated temperatures and pressures. VI. Raman studies of perchloric acid. *Can. J. Chem.* **1984**, *62*, 1134-1144.

(33) Sundberg, P.; Moyes, R. B.; Tomkinson J. Inelastic neutron scattering spectroscopy of hydrogen adsorbed on powdered-MoS_2, MoS_2-Alumina and Nickel-Promoted MoS_2. *Bull. Soc. Chim. Belg.* **1991**, *100*, 967-976.

(34) Pennella, F. Tetrahydrido-complexes of molybdenum. *J. Chem. Soc. D* **1971**, *3*, 158a-158a.

(35) Green, M. L. H.; Silverthorn, W. E. Arene molybdenum chemistry: some π-allyl, hydrido, and dinitrogen derivatives. *J. Chem. Soc. D* **1971**, *11*, 557-558.

(36) Deng, Y.; Ting, L. R. L.; Neo, P. H. L.; Zhang, Y.-J.; Peterson, A. A.; Yeo, B. S. Operando Raman spectroscopy of amorphous molybdenum sulfide (MoS_χ) during the electrochemical hydrogen evolution reaction: identification of sulfur atoms as catalytically active sites for H^+ reduction. *ACS Catal.* **2016**, *6*, 7790-7798.

Table of Contents artwork